JOURNAL OF MATERIALS SCIENCE 17 (1982) 517–524

Initiation of mode I degradation in sodium-beta alumina electrolytes

L. A. FELDMAN*, LUTGARD C. DE JONGHE
Materials and Molecular Research Division, Lawrence Berkeley Laboratory and Department of Materials Science and Mineral Engineering, University of California, Berkeley, California 94720, USA

The extension of initial surface cracks by the focusing of the ionic current in beta alumina electrolytes (Mode I degradation) is discussed in terms of existing models. Focusing for an ion current impinging on an elliptic-cylindrical flaw is calculated by solving for the electric potential with suitable boundary conditions. The current density distribution along the crack is used to calculate the sodium flow velocity and Poiseuille pressure inside the flaw. Calculated critical current densities using a K_{Ic} criterion are several orders of magnitude higher than measured average critical current densities. This implies a lower effective K_{Ic} for electrolytic degradation than for mechanical testing. Current density enhancement around insulating barriers, such as non-wetted surface areas, is also calculated using elliptic- cylindrical coordinates. Significant current density enhancements are found, but they are localized in very small regions. Crack growth would occur within these regions, but should be arrested once the flaw extends past the high current density zone. A plausible mechanism for decreasing K_{Ic} in the electrolytic case is discussed.

1. Introduction

The degradation of sodium–β and β'' alumina fast ion conductors during cycling in sodium/sulphur cells may occur by different mechanisms [1]. Mode I degradation is the penetration of the electrolyte by a sodium-filled crack or crack network propagated through the electrolyte from the sodium/β alumina interface, driven by cathodic plating of sodium into the crack. In contrast to Mode I, Mode II degradation results from the formation of sodium metal in the bulk of the solid electrolyte as a consequence of the development of some electronic conduction. For Mode I, the local cathodic deposition of sodium is enhanced by the crack geometry. A specific calculation requires the assumption of a specific crack geometry. As was indicated by De Jonghe *et al.* [2], this crack geometry may be complicated in the propagation phase where frequently crack branching may be observed. For the purpose of calculating current density thresholds for the initiation of Mode I failure, the assumption that a single, small, sodium-filled surface crack is the active defect appears to be quite plausible.

In the first treatment of the Mode I breakdown problem by Armstrong *et al.* [3], the electrolyte was modelled as a parallel sided slab with a sodium-filled flaw extending perpendicular to the sodium/electrolyte interface. The flaw was then considered to take the form of a hemispherically capped cylinder. The current flowing into the flaw was obtained by assuming the sodium metal to be at the same potential everywhere, and by calculating an effective resistance around the tip of the crack. This approximate treatment gave the qualitative result that the crack growth velocity is proportional to the crack length and to the average current density in the slab, but it did not make use of a critical fracture concept and did not yield a "threshold" current density below which degradation of this type will not occur.

A further analysis has been given by Shetty *et*

*Present address: Materials Sciences Laboratory, Aerospace Corporation, P.O. Box 92957, Los Angeles, California 90009.

0022–2461/82/020517–08$2.80/0

al. [4], in which the crack shape was calculated using elasticity theory such that its shape was consistent with the pressure generated due to the viscous flow of the sodium within. A crack profile–pressure distribution was then determined by an iterative calculation reaching self-consistent results. The finding was that the profile changed little after the first iteration, given an approximately parallel sided crack with rounded tip and a uniform pressure gradient. By incorporating the critical fracture concept together with the linear pressure profile, large current densities were calculated to be necessary for crack extension. The current densities were on the order of 1500 A cm^{-2} for an initial flaw length of 25 μm in β'' alumina. This is about a factor of 10^3 larger than the typical average current densities that are observed for the initiation of rapid breakdown by Mode I.

A more accurate treatment is given here for the current focusing and fracture problem, in that it calculates directly the primary current density distribution and sodium pressure along the crack. Some simplification in the analysis is achieved by using an elliptic-cylindrical crack shape. This further refinement of the current focusing problem leads to a critical current density that is even higher than the ones calculated in the more approximate treatments, necessitating the introduction of additional crack tip processes, such as metal deposition ahead of the crack tip.

2. Current focusing – sodium flow velocity

The calculation is performed for a crack of elliptic-cylindrical shape, as shown in Fig. 1. The equation $\nabla^2 \phi = 0$ is readily solved in elliptic-cylindrical coordinates in terms of elementary functions [5], and it remains only to tailor the boundary conditions fitting the present problem to determine the particular solution. The crack coordinate system and geometry are indicated in Fig. 2. The elliptic-cylindrical coordinates are defined by

$$\begin{aligned} x &= a \cosh \eta \cos \psi \\ y &= a \sinh \eta \sin \psi \\ z &= z. \end{aligned} \tag{1}$$

The crack parameters of length, l, and one-half the crack opening displacement, r, are given by

$$\begin{aligned} l &= a \cosh \eta_0 \\ r &= a \sinh \eta_0. \end{aligned} \tag{2}$$

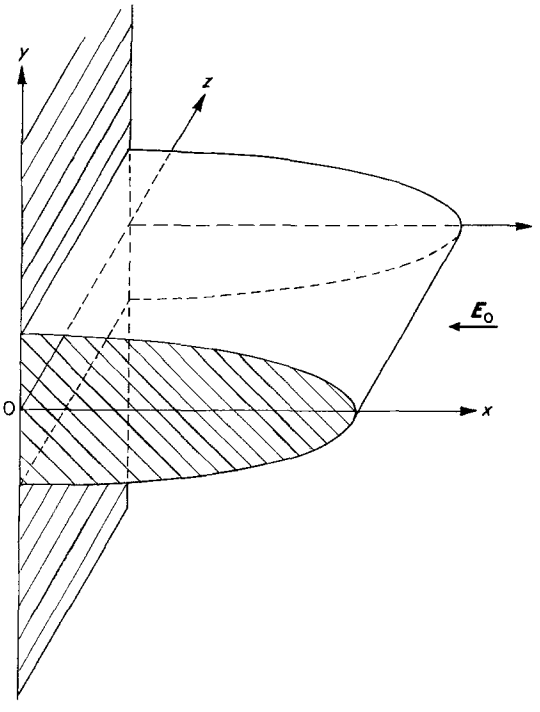

Figure 1 Current focusing geometry for elliptic-cylindrical crack.

The potential is chosen to satisfy the uniform field condition at infinity, $\phi = E_\infty x$, while at the sodium/electrolyte interface, $\phi = 0$. The potential inside the electrolyte is then found to be

$$\phi = \frac{E_\infty a \cos \psi}{\cosh \eta_0 - \sinh \eta_0} \times (\cosh \eta_0 \sinh \eta - \sinh \eta_0 \cosh \eta). \tag{3}$$

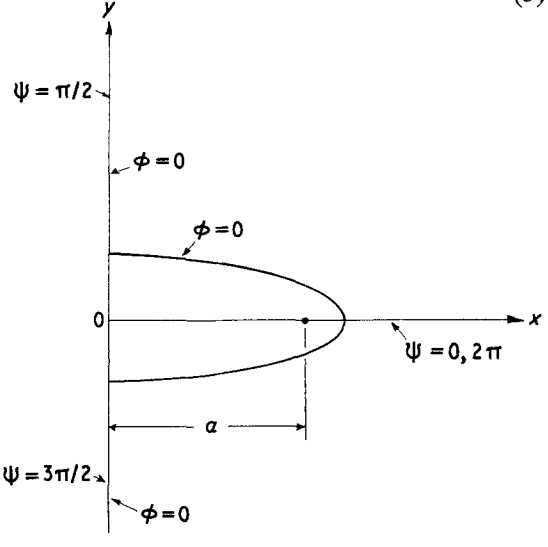

Figure 2 Co-ordinate system for elliptic-cylindrical crack.

The field is obtained from $\mathbf{E} = -\nabla\phi$ in elliptic-cylindrical coordinates. The current density flowing through the surface of the crack ($\eta = \eta_0$) is

$$j = \frac{j_\infty \cos\psi\,(\cosh\eta_0 + \sinh\eta_0)}{(\cosh^2\eta_0 - \cos^2\psi)^{1/2}} \tag{4}$$

where $j_\infty = \sigma E_\infty$.

The current density at the tip ($\psi = 0$) for a narrow crack ($r/l \ll 1$) is

$$\begin{aligned} j_{\max} &= j_\infty\,(1 + \coth\eta_0). \\ &\simeq j_\infty\, l/r \end{aligned} \tag{5}$$

This value is a factor of two smaller than the one obtained by the approximate treatments of Richman and Tennenhouse [6].

From the current density distribution, the total sodium flow as a function of distance along the crack can be found, yielding an average flow velocity that is independent of position along the crack. This is a consequence of the elliptic crack geometry and simplifies the calculation. The current contribution, $j(\psi)$, per unit width, w, along z for an element of arc along the crack surface is

$$\frac{\mathrm{d}i(\psi)}{w} = 2j(\psi)\,\mathrm{d}S, \tag{6}$$

where $\mathrm{d}S = a\,(\cosh^2\eta_0 - \cos^2\psi)^{1/2}\,\mathrm{d}\psi$.

The factor of 2 arises since the current is fed in from both sides of the crack. Substitution for $j(\psi)$ from Equation 4 and integration gives

$$i(\psi)/w = 2j_\infty\, a\,(\cosh\eta_0 + \sinh\eta_0)\int_0^\psi \cos\psi\,\mathrm{d}\psi,$$

or (7)

$$i(\psi)/w = 2j_\infty\, a\,(\cosh\eta_0 + \sinh\eta_0)\sin\psi.$$

The total current into the crack ($\psi = \pi/2$) per unit width is approximately $2j_\infty\, a$, which compares well with the estimate of Richman and Tennenhouse [6]. The flow velocity is related to the ratio of the flow through a cross section of the crack to the cross section area, $i(\psi)/2wy(\psi)$. This average flux $\bar{j}$ is given by

$$\bar{j} = \frac{j_\infty\,(\cosh\eta_0 + \sinh\eta_0)}{\sinh\eta_0}. \tag{8}$$

The flow velocity for sodium, $\bar{v}$, is determined from the relation $\bar{j} = ne\bar{v}$ where n is the atom number density of liquid sodium and e is the sodium ionic charge. Thus

$$\bar{v} = v_\infty\,(1 + \coth\eta_0) \tag{9}$$

where $v_\infty = j_\infty/ne$. Thus, the velocity, $\bar{v}$, is independent of position along the elliptic-cylindrical crack.

3. Flow pressure and fracture mechanics of crack

The flow pressure is calculated, assuming Poiseuille type viscous flow along x between infinite parallel plates of spacing $2y$

$$\frac{\mathrm{d}P}{\mathrm{d}x} = \frac{-3\tau\bar{v}}{y^2} \tag{10}$$

where τ is the viscosity and $\bar{v}$ is the average flow velocity. This will be in reasonable agreement with the present geometry away from the tip of a long, narrow crack with nearly parallel faces.

In the high curvature region at the tip, the flow will be more nearly perpendicular to the walls. The assumption that $\bar{v}$ is given by Equation 9 up to the crack tip should over-estimate the pressure gradient near the tip, thus giving an upper bound on the pressure. The gradient is

$$\frac{\mathrm{d}P}{\mathrm{d}x} = \frac{-3\tau v}{a^2\sinh^2\eta_0\sin^2\psi}, \tag{11}$$

or

$$\frac{\mathrm{d}P}{\mathrm{d}x} = \frac{-3\tau\bar{v}}{r^2\,(1 - x^2/l^2)}. \tag{11a}$$

Assuming $P = 0$ at $x = 0$, we integrate to find $P(x)$

$$P(x) = P_0\tanh^{-1}(x/l) \tag{12}$$

where $P_0 = -3\tau\bar{v}l/r^2$, which is the pressure head developed along a parallel sided channel of spacing $2r$. This is the pressure head value of Shetty *et al.* [4]. The two pressure distributions are compared in Fig. 3.

In terms of fracture mechanics approach, K_I must be evaluated for this internally loaded crack. It is given for an internally loaded edge crack [7] by

$$K_I = \frac{2}{\pi}\int_0^l \frac{[1 + f(x/l)]\,l^{1/2}\,P(x)\,\mathrm{d}x}{(l^2 - x^2)^{1/2}} \tag{13}$$

with $f(u) = (1-u)(0.2945 - 0.3912u^2 + 0.7685u^4 - 0.9942u^6 + 0.5094u^8)$. Equation 13 is an integral form of the formula for K_I given by Sih [7] for loading by a point force. Substitution of

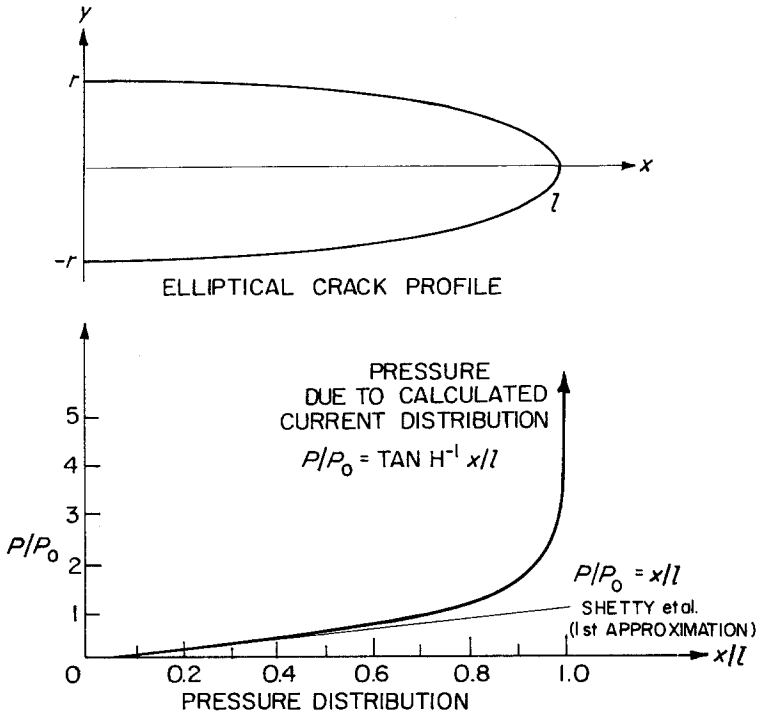

Figure 3 Comparison of calculated pressure distributions along crack.

$P(x)$ from Equation 12 reduces the problem to evaluating a series of convergent integrals of the form

$$\int_0^1 q^n (1-q^2)^{-1/2} \ln\left(\frac{1+q}{1-q}\right) dq \qquad (14)$$

which are transformed, by substituting $y = \ln (1+q)/(1-q)$, into integrals of the form:

$$1/2 \int_0^\infty \frac{y \tanh^n(y/2)}{\cosh(y/2)} dy \qquad (15)$$

These integrals can be approximated numerically using Simpson's rule. The results (for $r/l \ll 1$) is:

$$K_I = \frac{3.783\, l^{1/2} P_0}{\pi} ,$$

or

$$K_I = \frac{11.35}{\pi} \tau (l/r)^3 l^{-1/2} v_\infty . \qquad (16)$$

Some results from fracture mechanics on the relation of crack displacement to length in a generalized crack geometry [8] may be used to eliminate r from Equation 14. This yields (see Appendix A)

$$r = (4k/3)^{1/4} l^{3/4} \qquad (17)$$

where

$$k = \frac{2}{E'} \frac{11.35\tau}{\pi^{3/2}} v_\infty$$

and E' is the Young's modulus. This gives

$$K_I = 1.35\, E'^{3/4} (\tau v_\infty l)^{1/4} \qquad (18)$$

or

$$K_I = 1.35\, E'^{3/4} (\tau/ne)^{1/4} (j_\infty l)^{1/4} \qquad (18a)$$

and

$$j_{crit} = K_{Ic}^4 E'^{-3} ne/(3.32\tau l). \qquad (19)$$

An illustration of some typical values of the crack parameters are shown in Table I. The values of the constants used are $E' = 10^5$ MPa, $\tau = 0.34$ centi-

TABLE I Calculated values of l, j_∞ and K_I/K_{Ic}

l (μm)	j_∞* (A cm^{-2})	K_I/K_{Ic}†
10	0.1	0.025
	10	0.08
	1000	0.25
100	0.1	0.045
	10	0.14
	1000	0.45
1000	0.1	0.08
	10	0.25
	1000	0.8

*$j_\infty = K_I^4 E'^3 ne/(3.32\tau l)$
†$K_{Ic} \simeq 1.6$ MPa m$^{1/2}$ from Shetty *et al.* [4]

poise for sodium at 300° C, and $ne = 4.2 \times 10^9$ coul m^{-3}. For comparison the mechanically determined K_{Ic} is about 1.6×10^6 MPa $m^{1/2}$ [4]. As can be seen, the critical current densities for cracks of reasonable length are very high compared to the typical values that are observed for electrolyte failure by Mode I [4].

4. Current enhancement around a blocking region

The problem of current distribution around a blocking layer in a solid electrolyte has been described by Virkar *et al.* [9] using a mechanical analogue of the current flow problem. It may also be treated directly as in the previously discussed example by choosing a suitable geometry in which the Laplace equation may be solved. In this case, an example of a blocking layer would be a portion of the electrolyte/sodium interface which is non-conducting, such as a non-wetted region or an unfavorably oriented plate-like crystallite in the surface. An elliptic-cylindrical geometry for the insulating barrier can be used again, and the Laplace equation is solved in elliptic-cylindrical coordinates. The flaw geometry and current flow orientation are shown in Fig. 4. The coordinates and crack parameters are the same as in the earlier example. The field far from the platelet is parallel to the y-axis and the condition on the potential at infinity is $\phi = E_\infty y$. The other conditions are that $\phi = 0$ in the x-z plane ($\psi = 0, \pi$) and the normal derivative of the potential vanishes at the platelet surface, $\partial\phi/\partial\eta = 0$ where $\eta = \eta_0$. The potential inside the electrolyte is given by

$$\phi = \frac{E_\infty \sin\psi \,(\cosh\eta_0 \cosh\eta - \sinh\eta_0 \sinh\eta)}{(\cosh\eta_0 - \sinh\eta_0)} \tag{20}$$

from which the electric field and current density are determined directly. The magnitude of the current density normal to the electrolyte surface flowing across the x-z plane ($\psi = 0, \pi$) is

$$j_y = j_\infty \frac{\coth\eta \coth\eta_0 - 1}{\coth\eta_0 - 1} \tag{21}$$

The magnitude of the current density enhancement j_{max}, at the edge of the platelet ($\eta = \eta_0; \psi = 0, \pi$) is

$$\begin{aligned} j_{max} &= j_\infty (\coth\eta_0 + 1) \\ &\simeq j_\infty \, l/r \end{aligned} \tag{22}$$

This current density enhancement around the edge of the platelet is a factor of two smaller than the one obtained by Virkar *et al.* [9] from the mechanical analogue of the problem.

An illustration of the qualitative nature of the mechanical analogue for the current density can be made by comparing the tangential stress around an elliptical hole in a sheet under uniaxial tension and the tangential current density around an identical hole in a conducting sheet with a uniform current density at infinity in place of the uniaxial tension. Fig. 5 shows the comparison between the calculated normalized tangential stress, as given in Jaeger [10] and the normalized tangential current density around the hole calculated as described above for $r/l = 1/2$. We see that the

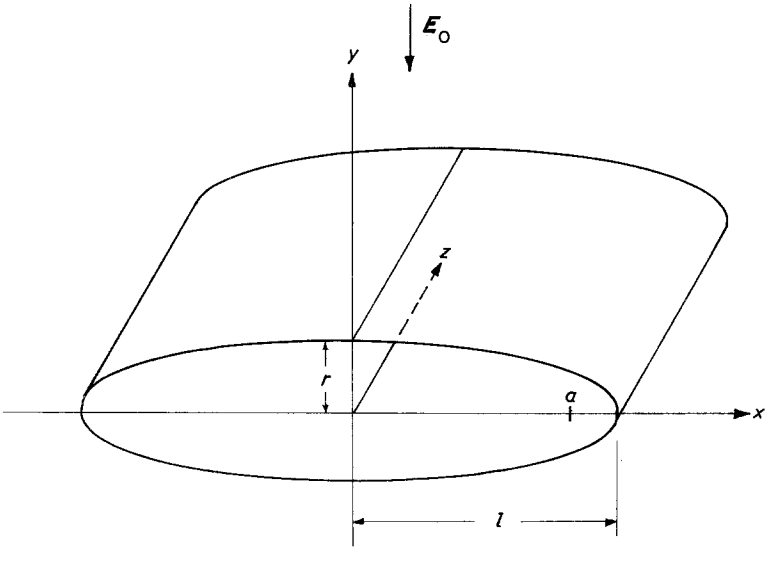

Figure 4 Geometry for elliptic-cylindrical blocking platelet.

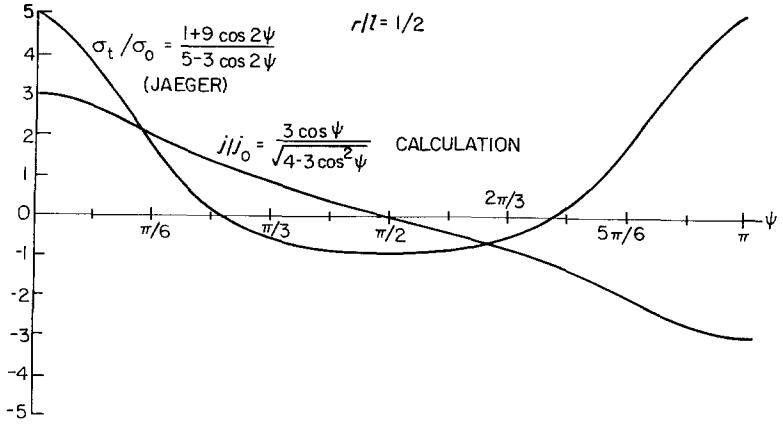

Figure 5 Comparison of current density and tangential stress around elliptical hole in sheet.

mechanical analogue is not exact in geometries such as these. For example, the calculated mechanical stress enhancement at the point of highest curvature around the hole shown in Fig. 5 is 5/3 times the electrical current density enhancement at the same point; the analogue tends to exaggerate the current density enhancement.

It is necessary to know the spatial extent of the zone of enhanced current density around the platelet. This allows an estimate of the increased current focusing experienced by an initial flaw situated at the edge of a platelet. From the relation of current density to position along the electrolyte/metal interface the maximum current density is found to occur at the platelet edge and to decrease smoothly to the value j_∞ far from the platelet. Let us now take the current density to be uniform in the current enhanced region, instead of decreasing, with a value of $j_{max} \simeq j_\infty l/r$. Let us also take the current density to be uniform outside the enhanced region, with a value of j_∞. Since the boundary condition of uniform current density of magnitude j_∞ at large y imposes a definite total current, the conservation of current (Kirchoff's Law) determines the width, R, of the high field or high current region. The total current in that region, $j_{max}Rw$, must be, to a first, approximation, $1/2(2j_\infty lw)$, for $r/l \ll 1$, which would be half the current flowing through the platelet area if the blocking platelet were removed. The current flowing around the platelet is in a sense a "displaced" current. Equating the current in the enhanced zone with the total displaced current gives a zone of width $j_\infty l/j_{max}$, or r. Thus, for $r/l \ll 1$ and large current density enhancement, the zone size is also very small compared to the length of the platelet. A somewhat more exact argument, which gives the same basic result can be made by finding the point of intersection of the tangents to the integrated current against position curve. The tangents to the curve are constructed at the platelet edge and at infinity, on the interface. Fig. 6 indicates schematically an initial flaw located at the edge of a blocking platelet in the enhanced current region.

Table II gives the values of j_{crit} for several assumed initial flaw lengths, L_c, and the approximate zone size, R, of the enhanced current density region near the platelet edge where the current density exceeds j_{crit}. The insulating platelet size was taken to be 1 cm, r/l was 10^{-7}, and j_∞ was 1 A cm^{-2}. The zone dimension, R, was estimated from a calculation of j_y using Equation 19. It could also be obtained from the approximation of Equation 19 since $j_y/j_\infty \simeq (l/2R)^{1/2}$, for $r/l < (2R/l)^{1/2} \ll 1$.

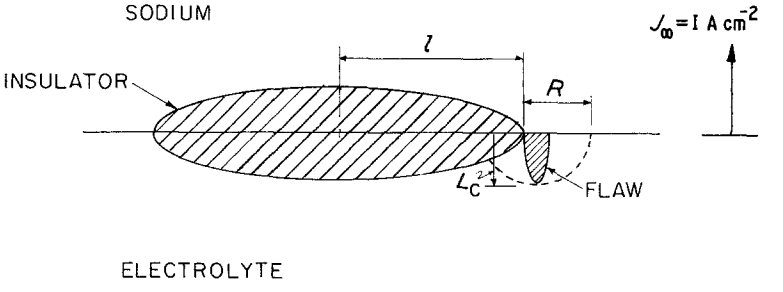

Figure 6 Metal-filled microcrack in enhanced current density zone.

TABLE II Microcrack size, L_c, critical current density, j_{crit}, and critical zone size, for $j_\infty = 1$ A cm^{-2}, $l = 1$ cm, and $r/l = 10^{-7}$

L_c (μm)	J_{crit} (A cm^{-2})	R (μm)
10	2.5×10^5	8×10^{-8}
100	2.5×10^4	8×10^{-6}
1000	2.5×10^3	8×10^{-4}

It is seen that the current enhancement zones are many orders of magnitude too small, or that the experimentally observed critical currents of a few A cm^{-2} are many orders of magnitude lower than the calculated ones. The results thus indicate that the Mode I mechanism needs to be modified in order to account for the large discrepancy that exists between calculated and observed critical current densities. It is difficult to envisage that anomalously high viscosities for sodium (e.g., due to impurities or to some geometrical restrictions in the capillary channel) could account for the discrepancy; rather, the results indicate that the effective critical stress intensity factor, K_{Ic}^{eff} is not the same as the one that is appropriate for mechanical testing, K_{Ic}. The results require that K_{Ic}^{eff} is about equal to $0.1\,K_{Ic}$. Processes are, therefore, thought to occur at the crack tip that bring the critical stress intensity factor significantly below the mechanical K_{Ic}. One such process is the local injection of electrons from the sharp, sodium-filled crack tip. The field at the crack tip, E_0, is about $E_\infty l/r$. From the observations of De Jonghe *et al.* [2], it is clear that r can be as low as 1 nm. E_0 can thus easily reach local values of 10^5 V cm^{-1} (for $E_\infty = 10$ V cm^{-1} and $L = 10\ \mu$m), which may indeed lead to profuse local field injection of electrons. This process would introduce significant electronic conductivity in the ceramic in the immediate vicinity of the crack tip, leading to sodium deposition under pressure just ahead of the crack tip [1]. This effect could lead to crack growth at some critical field that is reached when the macroscopic current density is well below the one at which the mechanical stress intensity factor K_I would exceed the critical stress intensity factor, K_{Ic}.

Acknowledgements

This work was supported by the Electric Power Research Institute. Additional support was received from the Assistant Secretary for Conservation and Solar Energy, Office of Advanced Conservation Technology, Electrochemical Systems Research Division of the U.S. Department of Energy under Contract Number W-7405-ENG-48.

Appendix

The crack opening displacement is calculated using a method based on the Theorem of Castigliano [8]. Fictitious forces, P, are applied to opposite sides of the crack and later set to zero at the location where the crack opening displacement is to be calculated. The forces are applied in this case at the opening of the elliptic-cylindrical crack. The displacement, r, is found to be

$$r = \frac{\partial \bar{U}_e}{\partial P} \tag{A1}$$

where $\bar{U}_e$ is the elastic strain energy and P is allowed to tend toward zero. $\bar{U}_e$ is expressed in terms of the previously calculated K_I and the stress intensity factor due to the fictitious forces. The total stress intensity factor is

$$K_I' = K_I + \frac{P}{(\pi l)^{1/2}} \tag{A2}$$

$\bar{U}_e$ is found from the strain energy release rate, G,

$$\bar{U}_e = \int_0^l G\,dl \tag{A3}$$

Using the relation between K_I and G (plane strain)

$$G = \frac{K_I'^2}{E'} \tag{A4}$$

we have

$$\bar{U}_e = \frac{1}{E'} \int_0^l \left(K_I + \frac{P}{(\pi l)^{1/2}} \right)^2 dl \tag{A5}$$

Using Equations A1 and A5, differentiating and setting $P = 0$ before integrating,

$$\begin{aligned} r &= \frac{2}{E'} \int_0^l \left(K_I + \frac{P}{(\pi l)^{1/2}} \right) (\pi l)^{-1/2}\, dl \\ &= \frac{2}{E'} \int_0^l \frac{K_I}{(\pi l)^{1/2}}\, dl \end{aligned} \tag{A6}$$

To find $r(l)$ from Equation A6, we note that r is on both the left side and the right side of the equation inside the integral, since Equation 16 shows that

$$K_I = \frac{11.35}{\pi} \tau \left(\frac{l}{r} \right)^3 l^{-1/2} \frac{j_\infty}{ne}$$

We then differentiate both sides of A6 with respect

to crack length and get a result of the form

$$\frac{dr}{dl} = kl^2 r^{-3} \tag{A7}$$

where k is a constant equal to

$$\frac{2}{E'} \frac{11.35\tau}{\pi^{3/2}} \frac{j_\infty}{ne}.$$

The solution to A7 is

$$r = \left(\frac{4K}{3}\right)^{1/4} l^{3/4} \tag{A8}$$

References

1. L. C. De JONGHE, L. FELDMAN and A. BUECHELE, *J. Mater. Sci.* **16** (1981) 780.
2. L. C. De JONGHE, L. FELDMAN and P. MILLETT, *Mater. Res. Bull.* **14** (1979) 589.
3. R. D. ARMSTRONG, T. DICKINSON and J. TURNER, *Electrochim. Acta* **19** (1974) 187.
4. D. K. SHETTY, A. V. VIRKAR and R. S. GORDON in "Fracture Mechanics of Ceramics" Vol. 4, Proceedings of the International Symposium on Fracture Mechanics of Ceramics, July 1977, University Park Pennsylvania, edited by R. C. Bradt *et al.* (Plenum Press, New York, 1978) pp. 651–665.
5. P. MOON and D. SPENCER, "Field Theory for Engineers", (D. Van Nostrand, Princeton, 1961) p. 202.
6. R. H. RICHMAN and G. J. TENNENHOUSE, *J Amer. Ceram. Soc.* 58 (1975) 63.
7. G. C. SIH, "Handbook of Stress-Intensity Factors", (Lehigh University Press, 1973) pp. 1.3.1–5.
8. S. TIMOSHENKO, "Strength of Materials", Part I, 3rd Edition, (D. Van Nostrand, Princeton, 1958) p. 328.
9. A. V. VIRKAR, L. VISWANATHAN and P. R. BISWAS, *J. Mater. Sci.* **15** (1980) 302.
10. J. C. JAEGER, "Elasticity, Fracture and Flow", (Methuen and Co., London, 1974) p. 189.

Received 6 April
and accepted 15 July 1981